Numerical Analysis of NREL 5MW Wind Turbine: A Study Towards a Better Understanding of Wake Characteristic and Torque Generation Mechanism

2016 J. Phys.: Conf. Ser. 753 032059

(http://iopscience.iop.org/1742-6596/753/3/032059)

Numerical Analysis of NREL 5MW Wind Turbine: A Study Towards a Better Understanding of Wake Characteristic and Torque Generation Mechanism

M Salman Siddiqui[1], Adil Rasheed[2], Mandar Tabib[2] and Trond Kvamsdal[1,2]

[1] Department of Mathematical Sciences, Norwegian University of Science and Technology, NO-7491 Trondheim, Norway
[2] SINTEF ICT, Department of Applied Mathematics, Postboks 4760 Sluppen, NO-7465 Trondheim, Norway

E-mail: muhammad.siddiqui@math.ntnu.no, adil.rasheed@sintef.no, mandar.tabib@sintef.no, trond.kvamsdal@math.ntnu.no

Abstract. With the increased feasibility of harvesting offshore wind energy, scale of wind turbines is growing rapidly and there is a trend towards clustering together higher number of turbines in order to harvest maximum yield and to leave a smaller footprint on the environment. This causes complex flow configurations inside the farms, the study of which is essential to making offshore wind energy a success. The present study focuses on NREL 5MW wind turbine with the following objectives (a)To compare Sliding Mesh Interface and Multiple Reference Frame modeling approaches and their predictive capabilities in reproducing the characteristics of flow around the full scale wind turbine. (b)To get a better insight into wake dynamics behind the turbine in near and far wake regions operating under different tip-speed-ratio and incoming turbulence intensities.

1. Introduction and objective

Research on the aerodynamic design of wind machines has played a significant role in the success of modern wind turbine technologies. This in turn contributed positively towards the success of wind energy against other renewable energy resources [1] as a result of which, a dramatic rise in the use of wind energy for clean electricity generation is observed during the past few decades. A Horizontal Axis Wind Turbine (HAWT) is one of the best and cleanest wind machine to convert kinetic energy in the wind into mechanical energy [2]. During the conversion, turbine blades are the prime contact with the incoming wind, therefore, efficient aerodynamic blade designs are considered as key to achieving peak efficiencies. A wind turbine is subjected to a wide range of operational conditions, the performance under which (like in [3]) needs to be evaluated. Currently, wind energy research is commonly conducted using experimental or numerical approaches. Experimental approach generally involves experimentation in wind tunnel using a scaled down model of the actual turbine or a full scale field experiment under real conditions. While the former suffers from a lack of scaling laws to extrapolate the findings in wind tunnel to a full scale, the later suffers from a lack of spatio-temporal resolution to make conclusions with confidence. Numerical modeling approach fills most of the shortcomings of the

experimental approach, if used appropriately, but it has been uncommon for full scale turbine so far because of the associated computational cost [4]. Fortunately, things are changing fast and with rapid advancements in computer technologies, modern supercomputers and numerical algorithms, such simulations are slowly becoming a norm. A numerical approach also gives more control over the specification of precise operational condition one expects the turbines to be subjected to (like incoming wind profiles, atmospheric stratification, turbulent intensities and tip-speed-ratio) and then probe quantity of interest at any location within the computational domain. Such investigations need large number of sensitivity studies therefore there is a need for computationally efficient yet accurate approach. To this end we start by comparing two different approaches to modeling rotating turbines: a computationally expensive but supposedly more accurate Sliding Mesh Interface (SMI) and a faster but less accurate Multiple Reference Frame (MRF). After having investigated the capabilities of MRF, it is used to evaluate the performance of a full scale turbine under different tip-speed-ratio (TSR) and inlet turbulent intensities (TI). Results are presented in the form of velocity deficits behind the turbine, torque vs TSR, torque vs TI, velocity field close to the blade sections and wake deficit behind the turbine.

2. Governing Equations

The flow around wind turbines, even the very large ones, is still essentially incompressible with Mach numbers, based on blade tip speed almost never exceeding 0.25. Hence, we have solved the incompressible form of Navier Stokes equation using a multiple reference frame (MRF) and Sliding Mesh Interface (SMI) approach. Using the MRF approach, in the current work, the computational domain is divided into two concentric zones: rotational and stationary with the former containing the rotating turbine. The governing equations are slightly modified to be compatible with the reference frame in which they are solved. In the stationary zone the following set of equations for mass and momentum are solved:

$$\nabla \cdot \mathbf{u_a} = 0 \tag{1}$$

$$\nabla \cdot (\mathbf{u_a} \otimes \mathbf{u_a}) = -\nabla p + \nabla \cdot (\nu + \nu_t)\nabla(\mathbf{u_a} + (\nabla \mathbf{u_a})^{\mathbf{T}}) \tag{2}$$

where $\mathbf{u_a}$ is the absolute velocity as seen from a stationary reference frame. In the rotating rotational zone the same equations are rewritten in terms of the relative speed $\mathbf{u_r}$ (relative to the rotating frame of reference) given by:

$$\nabla \cdot \mathbf{u_r} = 0 \tag{3}$$

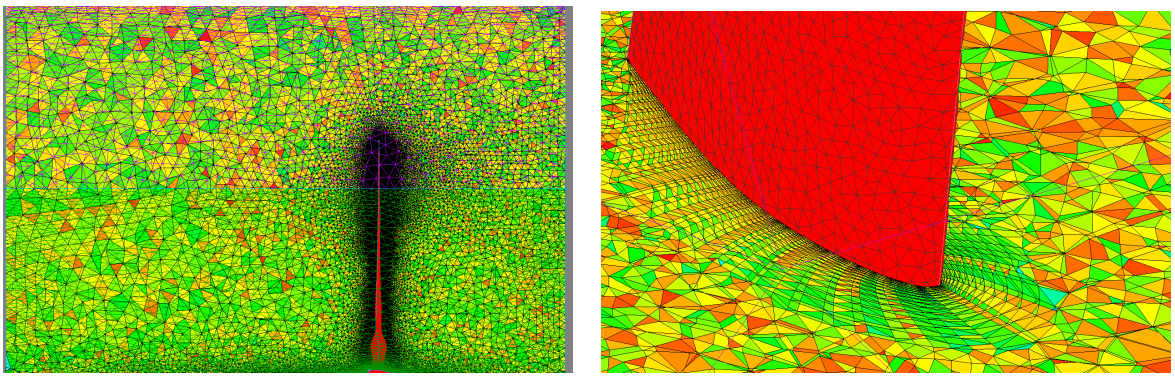

(a) Mesh (b) Zoomed in view

Figure 1. Computational mesh

$$\nabla \cdot (\mathbf{u_r} \otimes \mathbf{u_r}) + \mathbf{2\Omega} \times \mathbf{u_R} + \mathbf{\Omega} \times (\mathbf{\Omega} \times \mathbf{r}) = -\nabla p + \nabla \cdot (\nu + \nu_t)\nabla(\mathbf{u_r} + (\nabla \mathbf{u_r})^{\mathbf{T}}) \quad (4)$$

$$\mathbf{u_a} = \mathbf{u_r} + \mathbf{\Omega} \times \mathbf{r} \quad (5)$$

where $\mathbf{\Omega}$ is the rotational speed of the reference frame with respect to a stationary observer (here it will also be equal to the rotational speed of the turbine), p is pressure, ν is the kinematic viscosity of the air and ν_t is the turbulent kinetic viscosity. Since MRF computes a steady state solution, the temporal derivatives are ignored in the equations. For turbulence modeling, $k-\omega$ and $k-\epsilon$ models with standard wall functions are used.

At the interfaces between the two zones, a local reference frame transformation is performed to enable flow variables in one zone to be used to calculate fluxes at the boundary of the adjacent zone. Velocities and velocity gradients are converted from a moving reference frame to the absolute inertial frame using Equation 5. No such special treatment is applied for scalar quantities such as pressure, density, turbulent kinetic energy and dissipation rates.

In the SMI approach, the domain and the mesh quality used is similar to MRF, however, the turbine and mesh are made to rotate physically with time. The governing equations are solved only in inertial reference frame and temporal derivatives are introduced which include the transient effects. Following equations are solved throughout the domain for SMI approach using $k-\epsilon$ turbulence model with standard wall function:

$$\nabla \cdot \mathbf{u_a} = 0 \quad (6)$$

$$\frac{\partial \mathbf{u_a}}{\partial t} + \nabla \cdot (\mathbf{u_a} \otimes \mathbf{u_a}) = -\nabla p + \nabla \cdot (\nu + \nu_t)\nabla(\mathbf{u_a} + (\nabla \mathbf{u_a})^{\mathbf{T}}) \quad (7)$$

3. Approach and methods

3.1. CAD model

The 5MW NREL turbine consists of three $63m$ long blades defined in terms of cross sectional profiles (DU21, DU25, DU30, DU35, DU40 and NACA64) and twist angles at different locations away from the hub [5] [6]. The slight twist angle along the blade length helps in accommodating the variations in relative wind velocity from root to tip. A parametric CAD model of the blade is generated using the data provided in Table 1.

Table 1. Detail of airfoils used in the construction of CAD model

Airfoil profile	Thickness (t/c)	Distance from the center (m)	Chord (m)	Twist angle(^{o})
Cylinder1	100%	2.00	3.542	0.000
Cylinder2	100%	5.60	3.854	0.000
DU40-A17	40.50%	11.75	4.557	13.308
DU35-A17	35.09%	15.85	4.652	11.480
DU30-A17	30.00%	24.05	4.249	9.011
DU25-A17	25.00%	28.15	4.007	7.795
DU21-A17	21.00%	36.35	3.502	5.361
NACA64-A17	18.00%	44.55	3.010	3.125

Table 2. Variation of turbulent intensity

Turbulence intensity	Turbulent kinetic energy (k)	Turbulent dissipation energy (ϵ)	Turbulent dissipation rate (ω)
5%	0.30375	0.0013753914	0.0503115295
10%	1.215	0.0110031315	0.100623059
15%	2.73375	0.0371355688	0.1509345885
20%	4.86	0.088025052	0.201246118

3.2. Domain and Mesh

Since, all the simulations presented in this work are with a uniform inlet velocity profile, the axial symmetry of the flow is exploited to reduce the size of the domain to just a 120^o sector (Figure 2) including a single blade. A hybrid finite element mesh with structured hexahedral elements close to the blade surface and tetrahedral mesh elsewhere is used. While the former is used to model boundary layer in an accurate way and to have a better control over the y^+ (used according the wall function), the latter is used because of the convenience in using it for local refinements in an optimal way (Figure 1). The hybrid mesh also ensures a smooth transition from structured to unstructured mesh. The final mesh consists of three million mesh elements. As described earlier, the domain is divided into two zones: stationary and rotating separated by a non overlapping interface. The relative tolerance between the zone face is set low (≈ 0.0001) to make the interface boundary as tight as possible.

3.3. Boundary Conditions

Simulations are conducted for a uniform inlet velocity profile, applied on the inlet face and for different TSR. The TSR is changed by adjusting the rotational speed of the turbine. At

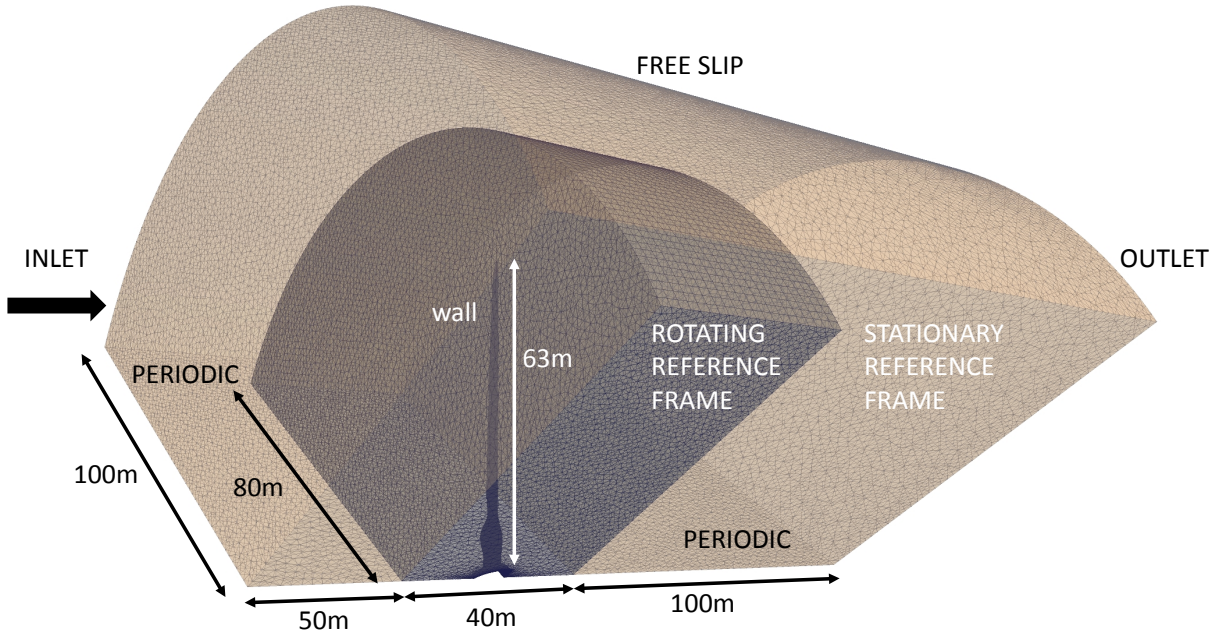

Figure 2. Domain and mesh

the outlet face a standard outlet boundary condition is used. A free slip boundary condition is applied on the curved surface. To impose axial symmetry, periodic boundary condition is applied on the adjacent faces. A no slip boundary condition is applied on the blade surface and wall function is used along with the $k-\epsilon$ and $k-\omega$ equations to work with relatively coarse mesh close to the blade surface. Figure 2 presents the boundary conditions applied on different faces.

3.4. Computational setup

For the base case used in [5],[7], reference fluid density $\rho = 1.225kg/m^3$, dynamic viscosity $\mu = 1.82 \times 10^{-5}kg/m.s$ and incoming wind velocity $U_\infty = 9m/s$ and turbine rotational speed $\Omega = 10rpm$ is used. Several more simulations are conducted with the same inlet velocity but with four different turbulent intensities (TI=5%, 10%, 15%, 20%) and seven different tip speed ratios (TSR=6, 6.5, 7, 7.7, 8, 8.5, 9). Table 2 gives more detail about the values of k, ϵ and ω. A self-adjusting time step based on a maximum Courant number of 1 is used to arrive at a steady state solution in case of MRF simulations. The solver is created in OpenFOAM-2.3.0 (OF). To ensure continuity, OF uses an elliptic equation for the modified pressure which involves combining the continuity equation with divergence of momentum equation. This elliptic equation along with the momentum equation and turbulence equation are solved in a segregated manner using the Semi-Implicit Method for Pressure-Linked Equations (SIMPLE) algorithm. The OF uses a finite volume discretization technique, wherein all the equations are integrated over control volumes (CV) using Green Gauss divergence theorem. The gauss divergence theorem converts the volume integral of divergence of a variable into a surface integral of the variable over faces comprising the CV. Thus, the divergence term defining the convection terms can simply be computed using the face values of variables in the CV. The face values of variables are obtained from their neighboring cell centered values by using convective scheme. In this work, all the equations (except k and turbulence equations) use second order linear discretization scheme, while the turbulent equations use upwind convection schemes. Similarly, the diffusion term involving Laplacian operator (the divergence of the gradient) is simplified to compute the gradient of the variable at the face. The gradient term can be split into contribution from the orthogonal and the non-orthogonal parts, and both these contributions are accounted for.

All the SMI computations are performed on 256 cores of a 2.6GHz Intel(R) Xeon(R) CPU machine ([8]) on $Vilje$, the high performance computational facility at Norwegian university of science and technology. THE MRF simulations are run with 8 cores on a 3.2 GHz Intel(R) Xeon (R) CPU machine.

4. Result and Discussion results

4.1. Validation study

Results for the base case is compared with the published results from NREL using FAST ([5], [7]) and with [9] using Variational Multi Scale (VMS). The two modeling approaches are on two extremities. While the FAST uses a simple Blade Element Method (BEM) to simulate the aerodynamics, the VMS approach is closer to a Large Eddy Simulation (LES) based models with capabilities to resolve most of the turbulence scales. Our RANS based approach with $k-\epsilon$, $k-\omega$ and SA lies somewhere in between since all the turbulence scales are modeled. From the Figure 4(b), in the absence of reliable observational data, it is difficult to say which method gives the most accurate prediction of the torque. Based on the three different turbulence models used in the simulations, a value of $\approx 2800kN-m$ for torque is obtained. All the three turbulence models predict roughly the same value of torque. Therefore, $k-\epsilon$ model is selected for subsequent analysis. SMI results with the $k-\epsilon$ model has shown good agreement with the MRF approach. This further strengthen the numerical accuracy of the present analysis. We investigate deeper into the numerical results obtained from different methodologies in the following subsections.

4.2. MRF vs. SMI

Both the methods employ rotational and stationary zones. The relative motion between the two zones gives rise to unsteady interactions (due to pressure waves that propagate and due to wakes). The SMI approach models such interactions and produces excellent results (see [1]). The MRF, on the other hand, solves for steady state and hence neglect the unsteadiness. To give an idea about the computational cost associated, we conduct one simulation with SMI on 256 cores of a 2.6GHz Intel(R) Xeon(R) CPU machine ([8]) and another simulation with MRF on a local desktop machine with 8 cores with 3.2 GHz Intel(R) Xeon (R) CPU's. Both the simulations have uniform inlet profiles of u, k, ϵ. The MRF simulation is run until a steady state solution is obtained. The SMI simulation is run to simulate one full rotation. Ideally, the simulation should have run for a few more rotations to completely eliminate the effects of initialization. The MRF simulation take 3 days as against the 7 days taken by the SMI simulation for only one rotation, making the former the choice for further analysis in this work.

For a quantitative comparison of the results, time averaged wake deficit from the SMI simulation is compared against the MRF steady state solution. The normalized wake deficit profile of wind velocity along the axial direction are plotted in the near wake region at a distance of 0.15R, 0.30R 0.45R, 0.60R, 0.90R and 1.30R from the turbine rotor (Figure 3). It is clear from the figure that close to the turbine ($\approx< 0.3R$) SMI technique show large variation in the wake as compared to away from the turbine ($\approx> 1R$). The eddies generated by the structure are highly oscillatory and contain more energy. This energy is advected and loses its concentration downwind of the turbine. Therefore, a large velocity deficit is observed close to the turbine. Another noteworthy, observation is a relative good agreement in the profiles away from the hub ($z > 0.5R$) and between $0.3R - 0.6R$ distance from the turbine along the direction of the flow. This can be attributed to the fact that flow remains attached to the blade cross sections located away from the hub while there are massive flow separations, vortex shedding and associated unsteadiness close to the hub.

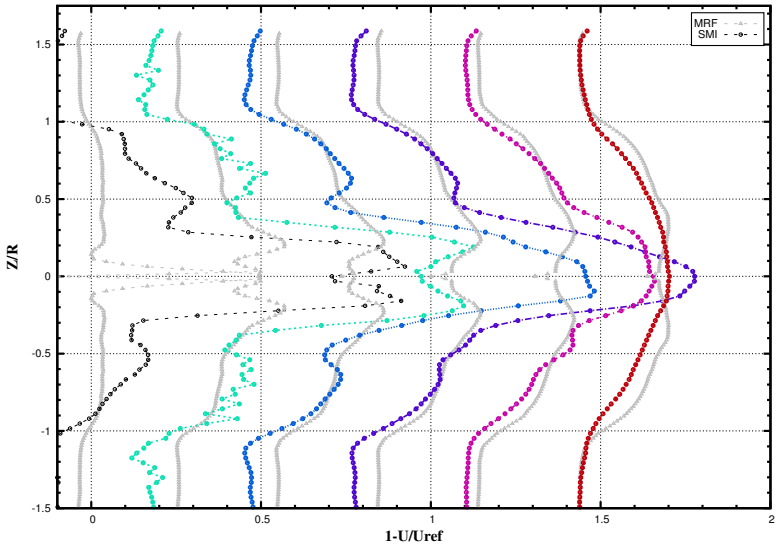

Figure 3. Velocity deficit behind the turbine for different tip-speed-ratio and at different locations (0.15R,0.30R,0.45R,0.60R,0.90R,1.30R from the hub). Note*: Successive profiles has been offset by a unit of 0.3 for better clarity.

4.3. Impact of Turbulent Intensity on torque generated
As mentioned earlier, four different values of turbulence intensity was used, the impact of which is presented in the Figure 4(c). It is clear from the figure that the torque generated increases slightly with an increase in the turbulence intensity at the inlet. However, the increase is insignificant after the TI is increased beyond 15%. This is an observation contrary to what was observed in the case of a vertical axis wind turbine ([3]).

4.4. Impact of TSR on torque generated
Figure 4(d) gives the variation of torque as a function of TSR. It indicates that the value of total torque first increases with TSR until it reaches a maximum (at TSR=7.5) and then starts to fall. This observation explains that it is important to understand the flow behavior at different sections of the blade in light of the cross sectional geometry. Close to the hub, in order to support the bulky turbine structures the geometry is rarely aerodynamic resulting in massive flow separation. The cross sectional geometry tends to get more aerodynamically shaped away from the hub and towards the blade edge. This is important since a big contribution of torque comes from the outer section of the blade. It is therefore important that the outermost section of the blade produces maximum torque which in turn requires two things firstly, there are no massive flow separations resulting in stall and secondly that the flow doesn't become symmetric

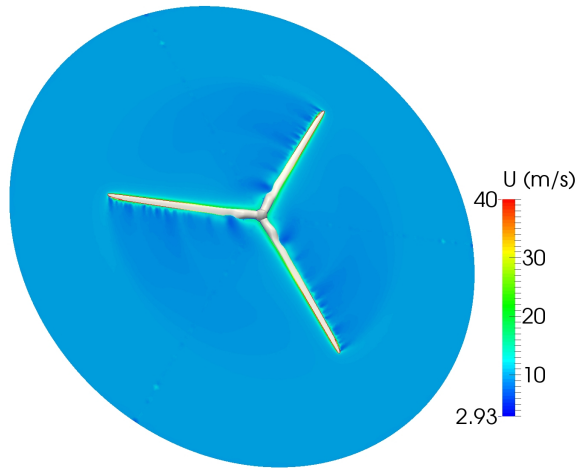

(a) Velocity contour on the plane containing the turbine

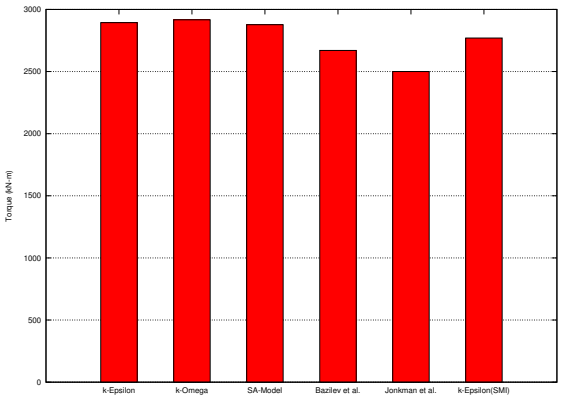

(b) Torque at TSR=7.5

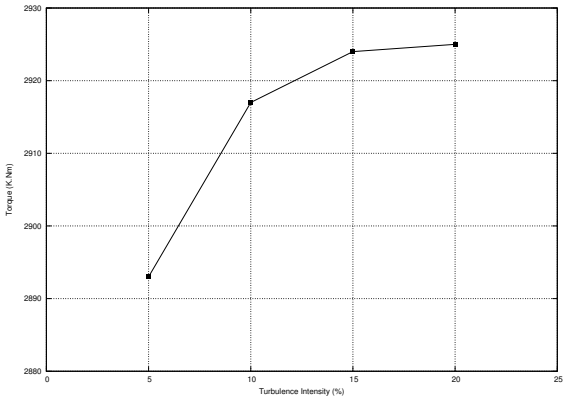

(c) Torque vs TI

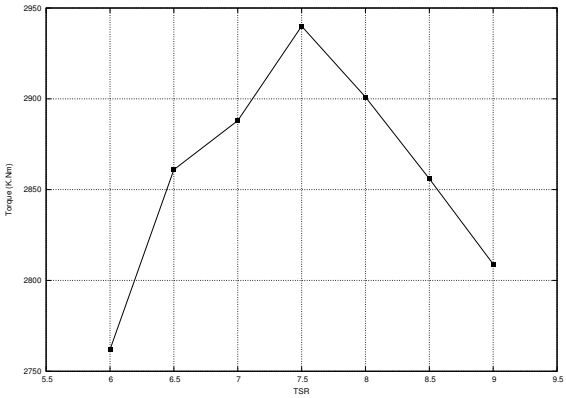

(d) Torque vs TSR

Figure 4. Simulated torque

relative to the blade. To achieve this, the twist angle is designed in such a way that at a particular TSR an angle of attack that generates maximum torque is achieved. See [10] for the variation of lift as a function of the angle of attack. Although, the referred work relates to NACA0012 blade, the same will be true for NACA64, which is the profile used in the outer section of the turbine blade under consideration. It appears from the figure 5(c) that the angle of attack relative to the moving blade is close to 15^o resulting in maximum lift and hence maximum torque contribution by this section. As TSR reduces, and reaches a value of 6.5 or 6, wind starts impinging on the top of the blade section instead of the leading edge, resulting in massive flow separation. This is true for all the cross sectional profiles along the blade length (see Figure 5(a) and 5(b)). The arrival of stall at lower TSR values than the optimal TRS value is the cause of under performance of a wind turbine at low TSR values. An opposite trend is observed when one approaches a TSR of 9. The flow becomes more symmetric relative to the blade and hence the lift generated diminishes resulting in a lower torque generation.

4.5. Velocity deficit

Plots of wake deficit ($\Delta U = 1 - U/U_\infty$) along the vertical line perpendicular to the axis of the turbine and on the downwind side at six locations (0.15R, 0.30R 0.45R, 0.60R, 0.90R, 1.30R) are shown in Figure 6. Each line in the plot corresponds to a wake deficit profile at a certain TSR value. It is observed that the wake deficit at every TSR gradually increases with the distance away from the rotor until 0.45R, after which the trend is reversed. The maximum wake deficit for sections located $< 0.6R$ is found at $\approx 20\%$ distance away from the turbine hub. Whereas, the location of maximum wake deficit for sections $>$ 0.6R has steadily displaced to $\approx 32\%$. At all sections, TSR=6 corresponds to the largest while TSR=9 corresponds to the lowest wake

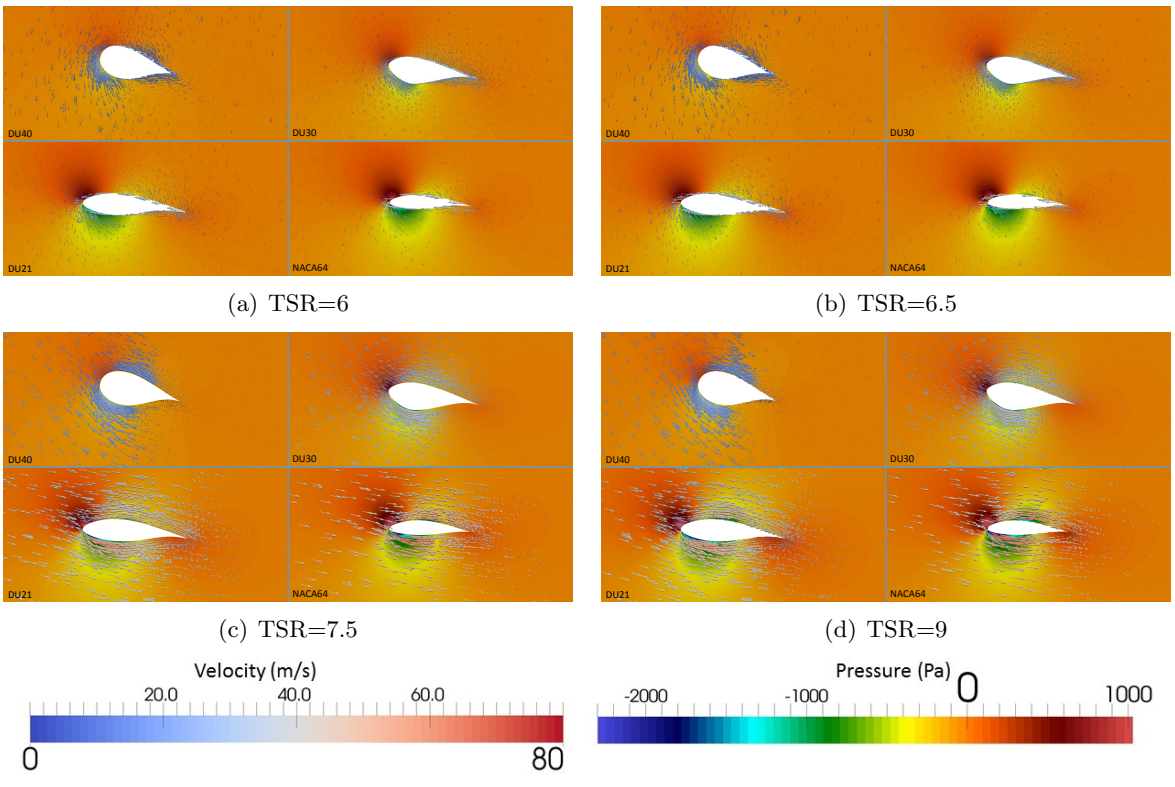

(a) TSR=6 (b) TSR=6.5

(c) TSR=7.5 (d) TSR=9

(e) Legend

Figure 5. Velocity vector and pressure contours at four different sections along the blade length

deficit, except at 0.15R, where the trend is opposite. Overall, the wake deficit has larger values adjacent to turbine center in comparison to the tip. The maximum wake deficit is observed at 0.1R distance in which a reduction of 40% is observed at all TSR values near the hub. Moving further downstream, the wake is found to have lost its variation, specially in areas near to the centerline of rotor. Sharp variations are observed to get diminish with the distance. In general, the trend for the wake deficit profiles having TSR value > 7.5 is almost similar. Where as, the profiles with values < 7.5 is found to be widely separated.

5. Conclusion and future work

Flow simulation around a full scale 5MW NREL reference turbine was conducted with SMI and MRF approach using $k - \epsilon$ turbulence model. Later the performance of the turbine operating at different tip-speed-ratio and incoming turbulent intensity were evaluated using MRF. The important findings are listed below:

- SMI has the ability to capture unsteadiness while MRF ignores it completely. This leads to a difference in their predictions closer to the hub where the flow is dominated by flow separation and vortex shedding.
- It is possible to use MRF on a desktop machine to do sensitivity analysis similar to the ones presented in the paper. The SMI approach requires supercomputing facility to provide fully converged results free from the effect of initializations.

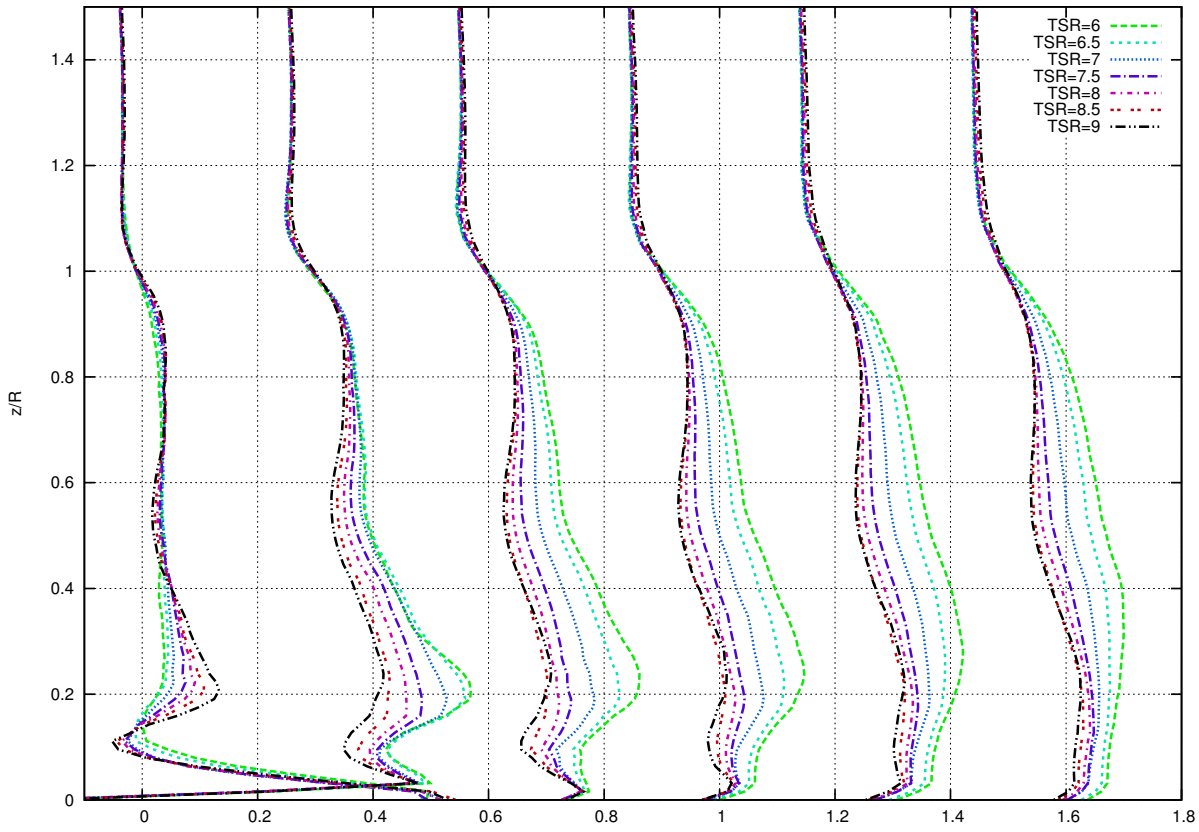

Figure 6. Velocity deficit behind the turbine for different tip-speed-ratio and at different locations (0.15R,0.30R,0.45R,0.60R,0.90R,1.30R from the hub). Note*: Successive profiles has been offset by a unit of 0.3 for better clarity.

- The turbine has optimal performance at a TSR of 7.5. Below this TSR, the performance degrades due to stall experienced by the outer sections of the blade. Above the optimal value of TSR, the incoming flow becomes symmetric relative to the blade section and this results in smaller magnitude of generated lift and hence the torque.
- There is little influence of the incoming turbulence intensity on the performance of a horizontal axis wind turbine.

In order to improve the understanding of flow characteristics behind a rotating turbine there is a need to validate the methodologies used in paper against experimental results. In the current work a RANS based $k-\epsilon$ turbulence model is used. The model is known to be inappropriate for simulations dominated by flow separation hence future studies will be undertaken using Large Eddy Simulations. When it comes to simulation of wind turbines in a wind farm, even the MRF approach will be computationally expensive. There will be a need for employing simpler models based on Strip Theory and Blade Element Method. Evaluation of their computational efficiencies and accuracies in comparison to SMI and MRF will also be undertaken in future works.

Acknowledgments

The authors acknowledge the financial support from the Norwegian Research Council and the industrial partners of NOWITECH: Norwegian Research Centre for Offshore Wind Technology (Grant No.:193823/S60) (http://www.nowitech.no) and FSI-WT (Grant No.:216465/E20)(http://www.fsi-wt.no). Furthermore, the authors greatly acknowledge the Norwegian metacenter for computational science (NOTUR-reference number: NN9322K/1589)(www.notur.no) for giving us access to the Vilje high performance computer at the Norwegian University of Science and Technology (NTNU).

References

[1] Siddiqui M S, Durrani N and Akhtar I 2015 *Renewable Energy* **74** 661 – 670
[2] Eriksson S, Bernhoff H and Leijon M 2008 *Renewable and Sustainable Energy Reviews* **12** 1419 – 1434
[3] Siddiqui M S, Rasheed A, Kvamsdal T and Tabib M 2015 *Energy Procedia* **80** 312 – 320 12th Deep Sea Offshore Wind Energy Conference, {EERA} DeepWind'2015
[4] Khalid S, Rabbani T, Akhtar I, Durrani N and Siddiqui M S 2015 *ASME Journal of Computational and Nonlinear Dynamics* **10** 041012(9)
[5] Jonkman J, Butterfield S, Musial W and Scott G 2009 *National Renewable Energy Laboratory* **Tech. Rep. NREL/TP-500e38060**
[6] Kooijman H, Lindenburg C, Winkelaar D and Hooft E 2003 *DOWEC Dutch Offshore Wind Energy Converter 1997-2003 Public Reports , DOWEC 10046-009, ECN-CX–01-135, Petten, the Netherlands: Energy Research Center of the Netherlands*
[7] Jonkman J, Marshal L and Buhl J 2005 *National Renewable Energy Laboratory, Golden, CO,* **Tech. Rep. NREL/EL-500-38230**
[8] *The Norwegian metacenter for computational science (NOTUR) http://www.sigma2.no.*
[9] Bazilevs Y, Hsu M C, Akkerman I, Wright S, Takizawa K, Henicke B, Spielman T and Tezduyar T E 2011 *International Journal for Numerical Methods in Fluids* **65** 207–235
[10] Nordanger K, Holdahl R, Kvarving A M, Rasheed A and Kvamsdal T 2015 *Computer Methods in Applied Mechanics and Engineering* **284** 664 – 688 isogeometric Analysis Special Issue